

Investigation of North Pacific Sea Ice Anomalies in the Context of Atmospheric and Oceanic Variability

Submitted by: Adrienne Tivy

July 19, 2001

Abstract

This study investigates the main mode of variability in North Pacific sea ice and examines the statistical relationship between ice extent and northern hemisphere climate variability for the period 1968-1997. Through empirical orthogonal function (EOF) analysis, correlations, and composite analysis, it was found that the seesaw pattern (first EOF of wintertime sea ice concentrations) between ice concentrations in the Bering Sea and the Sea of Okhotsk, generally used to characterize North Pacific sea ice, does not adequately address variability in the Sea of Okhotsk. Strongest correlations between the principal component timeseries of the first EOF and SLP and 500mb heights, occur with the atmosphere lagging the ice, suggesting anomalous geostrophic winds force the sea ice anomalies.

Relationships between the the sea ice dipole and the large scale circulation change during the 1977 and 1989 regime shifts in the North Pacific climate. Before 1977 the dipole is strongly related to Tropical variability and is correlated to the El Nino Southern Oscillation (0.62). Between 1977 and 1989, the dipole is strongly related to mid-latitude variability and is correlated with the Pacific Decadal Oscillation (0.62). After 1989 ,the dipole is also related to mid-latitude variability but the correlation with the PDO is opposite in sense (-0.72). All three periods show evidence of a Eurasian snow forcing of the sea ice through changes in the position and strength of the Siberian High.

Abstract

This study investigates the main mode of variability in North Pacific sea ice and examines the relationship between sea ice concentration and northern hemispheric climate variability for the period 1968-1997. Through empirical orthogonal function (EOF) analysis, correlations, and composite analysis, it was found that the seesaw pattern (first EOF of wintertime sea ice concentrations) between ice concentrations in the Bering Sea and the Sea of Okhotsk, generally used to characterize North Pacific sea ice, does not adequately address variability in the Sea of Okhotsk. Strongest correlations between the principal component time series of the first EOF and SLP and 500mb heights, occur with the atmosphere leading the sea ice, suggesting the possible presence of both thermal and dynamic effects.

Relationships between the sea ice dipole and the large scale circulation change with the 1977 and 1989 regime shifts in the North Pacific climate. Before 1977 the dipole is strongly related to tropical variability and is correlated to the El Nino Southern Oscillation (SOI, 0.62). Between 1977 and 1989, the dipole is strongly related to mid-latitude variability and is correlated with the Pacific Decadal Oscillation (PDO, 0.62). After 1989, the dipole is also related to mid-latitude variability but the correlation with the PDO is opposite in sense (-0.72). All three periods show evidence of a Eurasian snow forcing of the sea ice through changes in the position and strength of the Siberian High.

Contents

1	Introduction	9
2	Data	12
2.1	Sea Ice Concentration	12
2.2	Sea Level Pressure and 500mb Height	13
2.3	Sea Surface Temperature	13
2.4	Snow Cover Data	13
2.5	Climate Indices	13
3	Methods	14
3.1	Correlations	14
3.2	EOF Analysis	15
3.3	Composite Analysis	16
4	North Pacific Sea Ice Variability	16
4.1	EOF Analysis	17
4.2	Other Statistical Analysis	18
4.3	Discussion	20
4.4	Relationship Between North Pacific Dipole and Large-Scale Circulation	22
5	North Pacific Sea Ice and Large-Scale Circulation	22
5.1	Correlation Patterns of SST	23
5.1.1	First Period (1968-1977)	25
5.1.2	Second Period (1977-1988)	26
5.1.3	Third Period (1988-1997)	26
5.1.4	Correlations in Remote Ocean Basins	27
5.2	Correlation Patterns of SLP	27
5.2.1	First Period	30
5.2.2	Second Period	30
5.2.3	Third Period	30
5.3	Correlation Patterns of 500mb Height	31
5.3.1	First Period	33
5.3.2	Second Period	33

5.3.3	Third Period	34
6	Eurasian Snow Effect	35
7	Synthesis	37
8	Conclusion	38
9	Appendix A: List of Abbreviations	42

List of Figures

1	Winter Sea Ice Concentrations in the North Pacific	9
2	Standard Deviation of North Pacific Sea Ice Concentrations	10
3	EOF1 of North Pacific Sea Ice Concentrations	10
4	PC1 Time Series	11
5	Time Series for PC1 and Sea Ice Indices	19
6	Correlation Patterns of Sea Ice Indices and PC1	21
7	Time Series of Climate Indices	23
8	Correlation Patterns of SST	24
9	Patterns of Average SLP	28
10	Correlation Patterns of SLP	29
11	Correlation Patterns of z500	32
12	Correlation Pattern of Snow Index and z500	36
13	Correlation Pattern of Snow Index and SLP	37
14	Origins of Possible Sea Ice Variability	39

List of Tables

1	PC1 Correlated with Sea Ice Indices	17
2	Composite Years for PC1 and Sea Ice Indices	18
3	Correlations of PC1 and Climate Indices	38

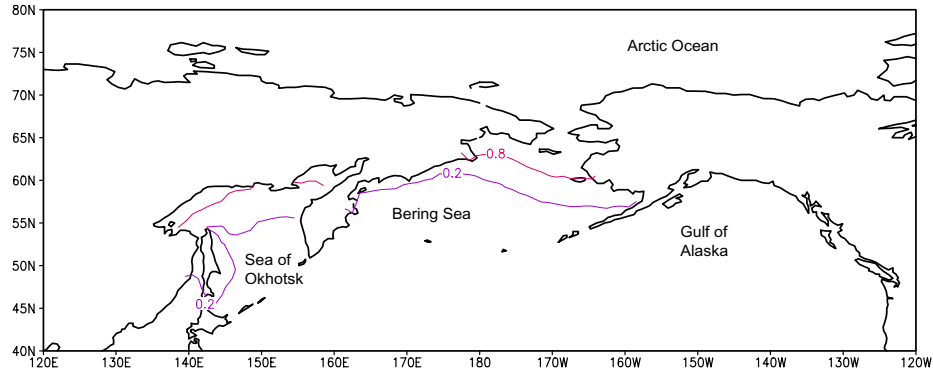


Figure 1: Winter Sea Ice Concentrations in the North Pacific
 Average wintertime (Jan-Feb-Mar) sea ice concentration in the North Pacific for 1968-1997. Contours shown are 20% and 80% coverage.

1 Introduction

Climate models and observational data suggest a poleward amplification of the effects of global climate change. One of the main causes is the albedo effect; as sea ice concentrations and snow cover decrease, less solar radiation is reflected at the poles causing the additional melting of sea ice or snow and thus leading to a positive feedback loop. It is for this reason that the study of Arctic sea ice has come to the forefront of climate change research. One of the main challenges facing climate change researchers is differentiating between natural climate variability and anthropogenic climate variability in order to predict how the climate may change as a result of global warming. This study focuses on understanding natural variability of North Pacific sea ice and its relation to the large scale climate.

North Pacific sea ice is the largest body of annual sea ice in the Northern Hemisphere, reaching a maximum coverage of $2 \times 10^6 \text{ km}^2$ (Cavalieri and Parkinson, 1987) in winter. Figure 1 shows the wintertime mean sea ice concentration in the North Pacific averaged over the months January, February and March. The annual life-cycle of sea ice in both the Sea of Okhotsk and the Bering Sea is quite similar. Ice growth begins as early as October and by December the ice edge is advected until it reaches its thermodynamic limit with maximum ice extent in March or April. In the Sea of Okhotsk, the ice advances towards the south-east with prevailing northwesterly winds, while in the Bering Sea, it is advected southward by northerly winds. Atmospheric forcing of Arctic sea ice was studied in detail by Thorndike and Colony

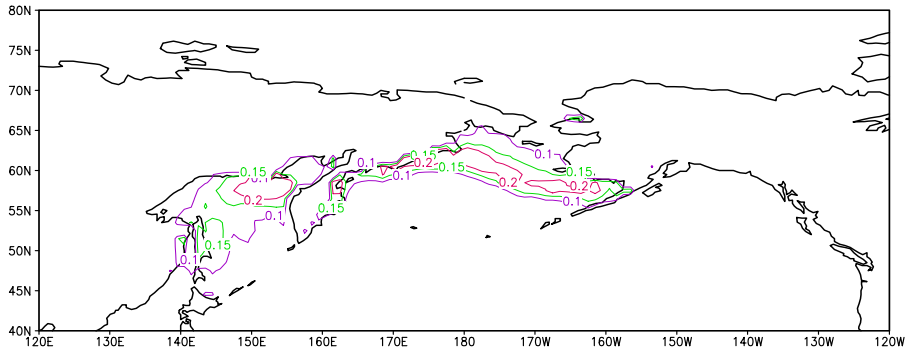


Figure 2: Standard Deviation of North Pacific Sea Ice Concentrations
 Wintertime (JFM) standard deviation for the gridded sea ice data set 1968-1997.

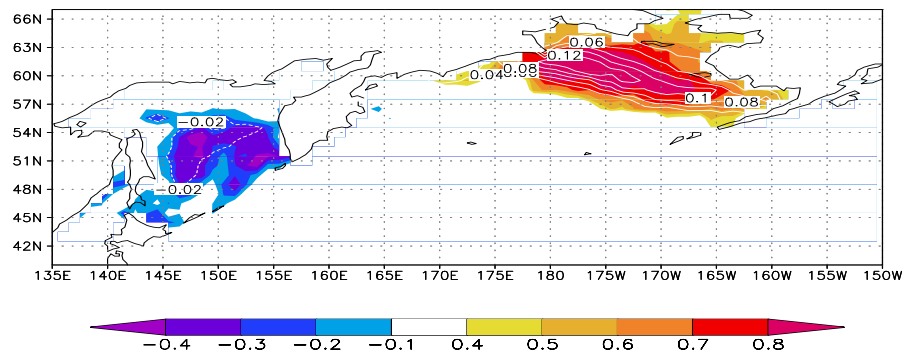


Figure 3: EOF1 of North Pacific Sea Ice Concentrations
 First EOF of wintertime sea ice (JFM) concentration for the period 1968-1977 which explains 27% of the total variability.

(1982) through the deployment of data buoys in the Arctic Ocean. They found that sea ice can respond to geostrophic winds in only a few days. The sea ice is advected at a speed of approximately 2% of the wind speed at an angle of 45 degrees to the right of the wind direction (Thorndike and Colony, 1982).

The main mode of variability in North Pacific sea ice has been identified as a seesaw pattern with opposing centers of action in the Sea of Okhotsk and the Bering Sea (Overland and Pease, 1982) (Figures 3 and 4). The dipole has surfaced as the dominant sea ice pattern in the visual inspection of sea ice concentrations in two week periods (Cavaliere and Parkinson,

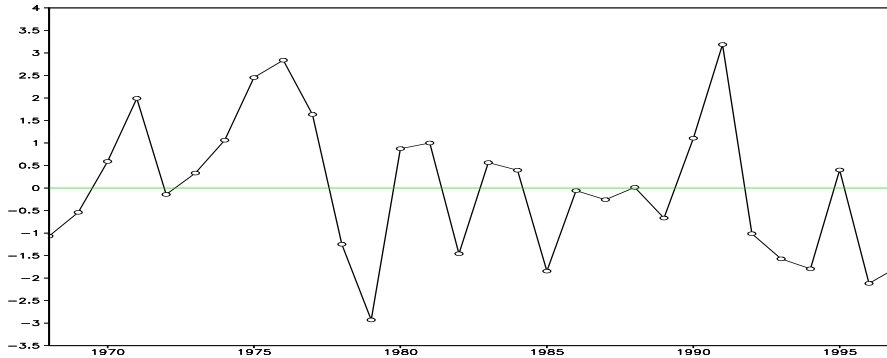


Figure 4: PC1 Time Series

Time series for the first principal component (PC1) from the EOF analysis. The units of the PC are arbitrary.

1987), Singular Value Decomposition analysis (SVD) (Fang and Wallace, 1994) and Empirical Orthogonal Function analysis (Deser et al. 2000; Fang and Wallace, 1998). All of these studies found the highest correlations between sea ice and sea level pressure when the sea ice lags by 1-4 weeks, consistent with anomalous geostrophic wind forcing of the sea ice anomalies. Comparisons between the EOF pattern and wintertime (JFM) variance in the sea ice data set (Figure 2) shows that the centers of action in the dipole pattern correspond with the location of the changing ice edge from year to year in the Bering Sea. However, in the Sea of Okhotsk, the variance in the wintertime sea ice (Figure 2) is highest for the ice edge off the north coast due to the southward winds, while the EOF pattern (Figure 3) captures the ice edge off the south western coast of the Sea of Okhotsk.

Fang and Wallace (1994) examined North Pacific sea ice for the period between 1972 and 1989. They found that one phase of the sea ice dipole is associated with a blocking high over Alaska, however, the 500mb height pattern associated with the dipole did not resemble any northern hemisphere teleconnection pattern. On the other hand, using SVD analysis, Fang and Wallace (1998) found that the sea ice dipole is highly correlated with the West Pacific pattern. The West Pacific pattern is the dominant mode of low frequency variability in Northern Hemisphere 500mb heights; it's main feature are two opposing centers of anomalous heights, one off the coast of Japan which extends across the Pacific ocean and another centered over the Bering Sea and the Sea of Okhotsk. Cavalieri and Parkinson (1987) examined the intra-annual variability in North Pacific sea ice. Using a Fourier analyzed SLP field, they were able

to link individual dipole events to changing positions and strengths of the Aleutian Low and the Siberian High.

It is widely accepted that the atmosphere-ocean coupled system in the North Pacific underwent a regime shift in 1977 (Trenberth and Hurrell, 1993; Hurrell, 1996; Mantua et al., 1997). In this context, a regime shift is defined as a shift in the mean state of the climate; the shift occurred over one year while the mean state of the climate persisted for over a decade. Changes in the atmospheric circulation associated with the 1977 regime shift include an eastward shift and deepening of the Aleutian low during the winter season which advects warmer air over North America and Alaska and cooler air over the North Pacific. The most notable changes in the ocean were cooler sea surface temperatures in the central North Pacific and warmer sea surface temperatures along the coasts of North America and Alaska.

There is debate over another possible regime shift in the North Pacific climate during the winter of 1989. This shift has been noted in the Arctic Oscillation and in sea ice variability in the Sea of Okhotsk (Tachibana, 1996), however, evidence for this regime shift is most striking in biological indicators (Hare and Mantua, 2000). A question that has yet to be addressed in the literature is the impact these regime shifts may have on the relationship between North Pacific sea ice and the large scale circulation. As such, this study sets out to address three main questions:

- How good is the dipole as a representative of sea ice variability in the North Pacific on inter-annual timescales?
- Can variations in the sea ice data set be related to large-scale atmospheric and oceanic variability?
- Do the suggested 1977, 1989 regime shifts influence the relationships between sea ice and Northern Hemisphere climate dynamics?

2 Data

2.1 Sea Ice Concentration

The UK Meteorological Office's (UKMO) GICE data set of global sea ice coverage was used in this study. The data is derived from Walsh's Sea Ice Concentration data set and com-

plex statistical analysis was used to produce global coverage on a 1-degree grid for the period 1871-present [Rayner et al., 1996]. The data set can be ordered from the following website, www.badc.rl.ac.uk/data/gisst/. Ice extent in the Sea of Okhotsk before 1968 is highly dependent on interpolations and as a result displays very little interannual variability. For this reason sea ice data before 1968 was not included in this analysis.

2.2 Sea Level Pressure and 500mb Height

Sea level pressure (SLP) and 500mb height (z500) gridded data sets are from the NCEP/NCAR 40-year Reanalysis Project (Kalnay et al., 1996). Both data sets are in the most reliable class of data in the analysis because they are strongly influenced by observations as opposed to model results. The data for SLP and z500 is available as monthly averages for the period 1958-1997 on 2.5 x 2.5 degree grids.

2.3 Sea Surface Temperature

The Reconstructed Reynolds Sea Surface Temperature (SST) data was provided by the NOAA-CIRES/Climate Diagnostic Center, Boulder, Colorado from their web site at <http://www.cdc.noaa.gov/>. This observational data set, which uses both in-situ and satellite measurements, was reconstructed using spatial and temporal patterns from empirical orthogonal functions (EOF) (Reynolds et al., 1995; Smith et al., 1995). Monthly data for the period 1968-1997 available on a 2-degree grid were extracted for this study.

2.4 Snow Cover Data

Data for Northern Hemisphere snow cover was provided by the NOAA-CIRES Climate Diagnostics Center from their website at www.cdc.noaa.gov/cdc/data.snowcover.html. The data set is presented as monthly percent snow cover, for the period 1971-1995, and is based on weekly snow charts derived from the visual inspection of visible-band satellite data. The data set has been interpolated to a 1x1 degree grid.

2.5 Climate Indices

An index of the Pacific Decadal Oscillation (PDO) was used to compare sea-ice variability with decadal variability in the North Pacific. The PDO index is from Nathan Mantua's website

at the University of Washington (<http://www.amos.washington.edu/~mantua/>). The PDO is defined as the leading principal component of SST anomalies in the North Pacific poleward of 20N. The SST data sets used in the PDO calculation are the UKMO Historical SST data set for the period 1968-1981, and the Reynolds Optimally Interpolated SST for the period 1982-1997.

The time series for the North Atlantic Oscillation (NAO) was obtained from the Climate Research Unit (CRU) of the University of East Anglia website (<http://cru.uea.ac.uk/data/nao.htm>). The index is the difference in normalized surface pressure anomaly between Ponta Delgada, Azores and Reykjavik, Iceland. In essence, the NAO is a measure of the strength of the westerly flow over the mid-latitude Atlantic Ocean.

The Arctic Oscillation (AO) index is from Baldwin and Dunkerton (1999), and is publicly available from Baldwin's website at www.nwra.com/resumes/mpb-res.html. The AO is defined as the first EOF of a single field comprised of 1000, 300, 100, 30 and 10 hPa heights. This definition of the index takes into consideration both tropospheric and stratospheric components of the polar vortex.

The Southern Oscillation Index (SOI) used in this study is from Data and Information Services at the Goddard Flight Center (Earth Sciences) from their website at www.daac.nasa.gov/FTP_SITE/readmes/soi.html. The data, constructed by the Climate Research Unit (CRU) at East Anglia University, is the difference in normalized sea level pressure between Tahiti, French Polynesia and Darwin, Australia.

3 Methods

3.1 Correlations

The main method of data analysis used in this study is correlations. By definition, correlation (Cor) is a measure of the covariability between two variables (X and Y) that is not dependent on scale:

$$\text{Cor} = \frac{\sum (x_i - \bar{x})(y_i - \bar{y})}{1/n \sum (x_i - \bar{x})^2 (y_i - \bar{y})^2}$$

where \bar{x}, \bar{y} = mean of time series

The correlation coefficient, Cor , is a value between 1 and -1, where a correlation of -1(+1) indicates a perfect linear relationship between the two variables, ie, $X=a+bY$, $b=[-1,1]$. Any value of b between -1 and 1 is a measure of the extent to which the two random time series vary linearly.

Correlations were used to elucidate the relationship between two single time series as well as a single time series and a gridded data set. For the analysis of gridded data sets, the correlation between the single time series and each grid point of the grid was calculated for the time dimension. The Student's t-test (Wilkes, 1995) was used to determine the significance of the correlations coefficient. The discussion focuses on correlations with a significance at the 95% level or greater.

3.2 EOF Analysis

Empirical Orthogonal Functions (EOFs) were analyzed to help characterize the main mode of variability in the sea ice gridded data set. EOF analysis is a technique used to identify patterns of variability. Identifying the mean and standard deviation of a data set does not give any insight into how variations in different geographic locations are correlated. In climate data sets a single point on the x-y plane is generally related to surrounding points. It is for this reason that EOF analysis is a popular statistical tool in climate analysis to compress information.

The variability of the sea ice data set was quantitatively determined from the auto-covariance matrix. In other words, the covariance between each pair of points in the x-y plane was calculated for the time dimension. The eigenvalues and eigenvectors of the covariance matrix were then calculated. The eigenvectors (a.k.a. empirical orthogonal functions) are the dominant patterns of variability; the eigenvalues (a.k.a. principal components, EOF time coefficients) display strength of the pattern over time.

In this analysis, both the spatial distribution of the variance (shaded regions shown as correlations between the PC and the full data) and the magnitude of the EOF pattern (contoured regions) are plotted. For the sea-ice data set approximately 50% of the variability is explained by the first two EOFs. Identifying a physical explanation for these two patterns is difficult because by definition all patterns of variability resulting from a single EOF analysis are orthogonal to one another. However, natural processes found in nature are generally related. For

this reason, EOF analysis is combined with composite analysis and correlations to elucidate the relationship between North Pacific sea ice and large scale climate variability.

3.3 Composite Analysis

Indices for winter averaged (JFM) sea-ice concentration in both seas were calculated to determine high and low ice years. Two approaches were taken. The first pair of indices were calculated using area averages over the whole sea, while the second used area averages over regions of high variability determined from the EOF analysis. Composite years were determined from these indices during the winter season using a cut-off value of one standard deviation from the mean.

Composite analysis was used to verify that the EOF patterns occur in reality and to help elucidate the relationship between wintertime sea ice concentrations and atmospheric variability. Because the period of record is only 30 years, composite analysis wasn't used to determine patterns in the large scale climate. With only a few composite years, high frequency variability is not filtered out by averaging, in fact, an extreme anomalous year would skew the composite averages.

4 North Pacific Sea Ice Variability

In order to understand the large-scale dynamics that influence annual sea ice concentration in the Bering Sea and the Sea of Okhotsk, it is important to first characterize sea ice variability in the two seas. To date, the main mode of inter-annual sea ice variability in the North Pacific has been identified as a dipole with opposing centers of action in the two seas (Cavalieri and Parkinson, 1987; Fang and Wallace, 1994, 1998; Deser et al., 2000). In other words, a year with above (below) average sea ice extent in the Bering Sea would be accompanied by below (above) average sea ice extent in the Sea of Okhotsk. Oscillating behavior in the climate system clearly characterizes inter-annual variability making it easier to explain in the context of the climate system as a whole. In this section the sea ice dipole is reproduced, but further analysis suggests it may not adequately represent interannual variability.

	PC1	Sea of Okhotsk	Bering Sea
PC1	0.29	-0.26	0.98(99)
Sea of Okhotsk	-	0.11	-0.23
Bering Sea	-	-	0.21

Table 1: PC1 Correlated with Sea Ice Indices

Correlations for PC1 and the sea ice indices at lag 0. Autocorrelations (diagonal boxes) of each index are calculated using a lag of one year.

4.1 EOF Analysis

The dipole pattern emerges as the leading eigenvector of winter averaged sea ice concentration in the northern hemisphere. In this study, the EOF was calculated using three month averaged (Jan-Feb-Mar) sea ice concentration in the North Pacific (40N-80N;120E-240E). These three months were chosen for the wintertime average because during this time the ice edge is being advected and a maximum ice concentration is reached in March.

The dipole pattern shown in Figure 3 explains 27% of the total variability in the data set and is consistent with previous studies (Fang and Wallace, 1998; Deser et al., 2000). The shaded regions represent the correlations between the PC1 time series and the gridded sea ice concentration data set. In the Bering Sea higher correlations, reaching a maximum of 0.8 are found, whereas, in the Sea of Okhotsk a maximum of only -0.4 is reached. The patterns and correlations are consistent with Panel 1 of Figure 6 where the same correlations are displayed in a slightly different format.

The contoured regions in Figure 3 show the amplitude of the dipole pattern. Multiplying the contours by the magnitude of PC1 for each year yields sea ice concentrations associated with the EOF pattern. Again, EOF1 appears to display greater variance in the Bering Sea where magnitudes reach a maximum of 0.12 compared to 0.02 in the Sea of Okhotsk. This is not consistent with Fang and Wallace (1998); the magnitudes of the EOF of sea ice concentration for the Sea of Okhotsk and the Bering Sea were equal in their study. Differences between the EOF patterns in these two studies could be attributed to the fact that in Fang and Wallace (1998) weekly sea ice data was used for the period 1972-1989 while in this study the period of record used is longer (1968-1997) and the EOF is based on monthly data.

Composite Years	High Ice Years	Low Ice Years
PC1	71,75,76,91	79,85,94,96,97
Bering Sea	71,75,76,77,91	79,82,85,94,96,97
Sea of Okhotsk	71,78,79,92,93,95	75,77,84,97

Table 2: Composite Years for PC1 and Sea Ice Indices

List of composite years derived from wintertime averaged (JFM) sea ice indices and PC1. A cut-off value of one standard deviation from the mean was used.

The time series for the first principal component (Figure 4) associated with the EOF pattern appears to be dominated by interannual variability with no visible trend. Low autocorrelations of PC1 (Table 1), that are not significant at the 95% confidence level, imply low memory from year to year. However, evidence of low frequency variability in the PC1 time series is seen in the composite years listed in line 1 of Table 2. Composite years calculated from the PC1 time series using a cut-off value of one standard deviation from the mean, show that almost all high ice years for the Bering Sea occur before 1977, while almost all low (high) ice years for the Bering Sea (Sea of Okhotsk) occur after 1977. The shift is not as striking in low ice years for the Sea of Okhotsk where only half of the low ice years fall before 1977.

4.2 Other Statistical Analysis

Because some of the statistical assumptions inherent in EOF analysis (see Methods Section 3) may cause results that have a statistical basis rather than the desired physical basis, it is important to explore variability in a data set using other methods. The total standard deviation at each point in the sea ice data set was plotted and compared to the EOF pattern (Figure 2). As in other studies, it was found that the centers of action in the two seas corresponds with the marginal ice zone (MIZ), the regions of highest variability, where the ice edge changes location from year to year. However, in the Sea of Okhotsk EOF1 and the plot of sea ice variance pick up different marginal ice zones. For the Bering, where the ice edge is advected from “north to south” (Cavalieri and Parkinson, 1987), this region is located in the northern part of the sea extending from Siberia to the eastern Aleutian Islands (Figures 2 and 3). For the sea of Okhotsk, where the ice edge is advected from “west to east” (Cavalieri and Parkinson, 1987), this region is located in the southern sea centered in the southern sea in the EOF (Figure 3) and off the northern coast in the contoured standard deviation plot (Figure 2).

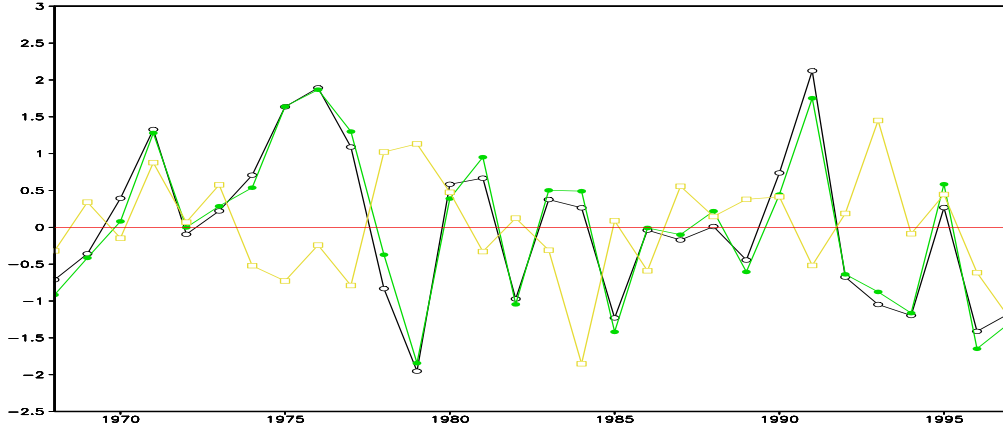


Figure 5: Time Series for PC1 and Sea Ice Indices

Time series for normalized PC1 (black), normalized wintertime (JFM) averaged Bering Sea ice concentration anomalies (green), normalized wintertime (JFM) Sea of Okhotsk average sea ice concentration anomalies (yellow). All time series have a standard deviation of 1.

While the plot of the variance at each point is consistent with the dipole pattern, composite analysis is not. Table 2 shows the high and low ice years for indices of sea ice concentration in both seas. The sea ice concentration index was calculated annually for the winter season (JFM), using area averages over each sea (Sea of Okhotsk: 45N-59N, 138E-158E; Bering Sea: 55N-64N, 168W-180W). As with PC1, composite years were identified using a cut-off of one standard deviation from the mean. High and low ice years for the Bering Sea are almost identical to the PC1 composite years while the composite years for the Sea of Okhotsk are very different. This analysis shows that the EOF pattern better explains variability in the Bering Sea than in the Sea of Okhotsk. This point is even more evident in Table 1 where correlations between the PC1 and both sea indices are compared.

In Figure 5, both sea ice concentration (shown as % coverage) indices and the time series for PC1 are normalized and plotted for comparison. The Bering Sea index closely follows PC1 while the Sea of Okhotsk index varies oppositely in some years but in others it varies in the same sense. A dipole relationship between the two sea ice concentration indices appears to be evident only intermittently.

Correlations between these time series are shown in Table 1. It was expected that if the relationship between the two seas was robust the two sea ice concentration indices would have a strong negative correlation, however, the correlation between the two indices is only -0.26. To check the robustness of this analysis, area averages calculated over the regions of highest variability in both seas were also calculated and correlated (not shown) and similar results were found.

The time series for PC1, the Bering Sea wintertime ice concentration index and the Sea of Okhotsk ice concentration index were all correlated with the wintertime (JFM) sea ice gridded data set for the 1968-1997 period. The results shown in Figure 6 support the notion that EOF1 is closely linked to variability in the Bering Sea and not the Sea of Okhotsk. The first panel is the correlation with PC1 and is therefore identical to the shaded regions in Figure 3. High correlations of up to 0.8 are found in the Bering Sea whereas the maximum correlations in the Sea of Okhotsk are only -0.4. The second two panels, for the Bering Sea index and the Sea of Okhotsk index respectively, show little relationship between sea ice concentrations in the two seas.

4.3 Discussion

Two main features of variability in the sea ice data set were examined in this section. The first was the dipole pattern that is routinely used to characterize the dominant mode of variability in North Pacific sea ice. EOF analysis supported the theory of an oscillating relationship between sea ice concentration in the Bering Sea and the Sea of Okhotsk. However, composite analysis using indices of sea ice concentration and correlation analysis suggests the dipole relationship is not robust and does not adequately address the dominant mode of variability in the Sea of Okhotsk.

The second feature examined was high and low frequency variability in the dipole pattern. While the time series for the first principal component of the EOF exhibited high interannual variability with low memory between years, there was evidence of low frequency variability, specifically, a shift in 1977 from above (below) to below (above) average sea ice concentrations in the Bering Sea (Sea of Okhotsk).

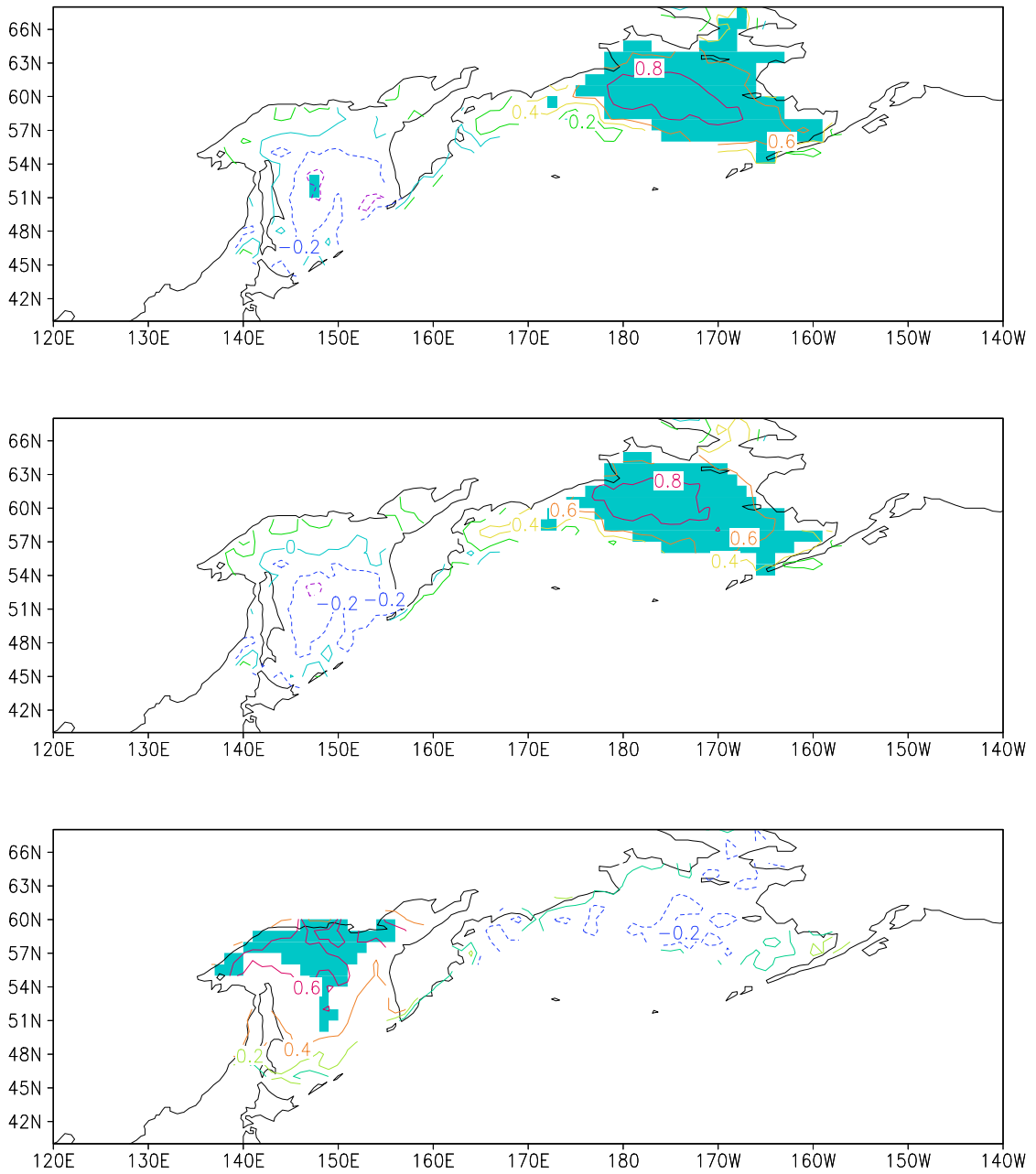


Figure 6: Correlation Patterns of Sea Ice Indices and PC1
 Correlations of wintertime (JFM) gridded sea ice data set with PC1 (top panel), the Bering Sea Index (middle panel) and the Sea of Okhotsk index for JFM (bottom panel). Shaded regions represent statistical significance at the 95% or greater level based on a t-test.

4.4 Relationship Between North Pacific Dipole and Large-Scale Circulation

To investigate the relationship between the dipole pattern and the large-scale circulation, the PC1 time series, for the period 1968-1997, was correlated with gridded data sets of sea level pressure, sea surface temperature and 500 mb heights. Additionally, lagged correlations were calculated to investigate lead-lag relationships between the atmosphere, ocean and sea ice. The PC1 time series (JFM) was kept constant while the gridded data set, using 3 month averages, were shifted six months from Oct-Nov-Dec to Apr-May-Jun. The largest correlations were found with the atmosphere and ocean leading by 1 month. Results are not shown because the significance of the correlations were low and no coherent large-scale features were revealed. The lack of significant results and strong correlations between the sea ice dipole and the SST, SLP and z500 fields was unexpected and prompted a new approach.

5 North Pacific Sea Ice and Large-Scale Circulation

When the principal component time series of the first EOF was correlated with SLP, SST and z500 at various lags over the entire time period (1968-1997), no large-scale climate patterns emerged. Because there was evidence of low frequency variability in the PC1 time series, in particular a shift in 1977, the possibility that the relationship between the large scale circulation and North Pacific sea ice varied over time was explored.

Figure 7 is a plot of the major northern hemispheric climate indices, averaged over the winter season (JFM) , for the period 1968-1997. The first panel shows the time series for the Arctic Oscillation (AO), followed by the time series for the North Atlantic Oscillation (NAO), the Pacific Decadal Oscillation (PDO) and the Southern Oscillation Index (SOI). The indices are smoothed using 9-point moving averages in order to highlight lower frequencies of variability.

The AO time series (Figure 7) showed both the 1977 and 1989 regime shifts; during the period 1977-1989 the AO is more frequently negative translating to a weaker polar vortex. The NAO time series (Figure 7) showed a large jump in the winter of 1989, from a more negative phase to a more positive phase. The PDO time series (Panel 3) displayed evidence of both regime shifts, after 1977 the PDO is in the positive phase with cool sea surface temperature anomalies in the North Pacific, after 1989 the index becomes negative for a few years and then is weakly positive. The SOI time series moves from more positive values, corresponding with cooler sea

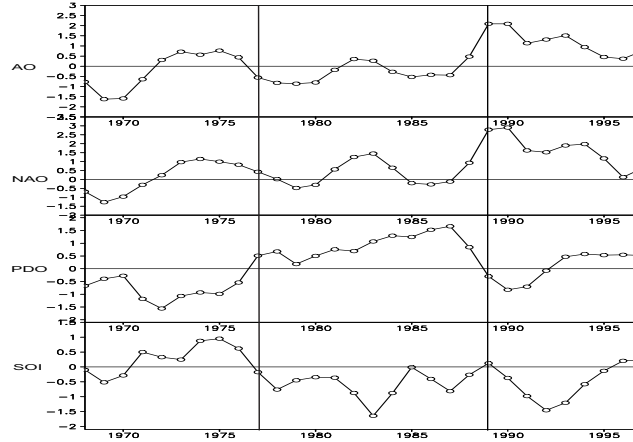


Figure 7: Time Series of Climate Indices

time series for the wintertime (JFM) climate index anomalies, calculated from the 30 year (1968-1997) mean, for the period 1968-1997. The top panel is the AO followed by the NAO, PDO and SOI. The 1977 and 1989 regime shifts are marked by vertical lines. The indices are normalized and have arbitrary units.

surface temperatures in the Topical Pacific (La Nina), to more negative values (El Nino) after 1977.

The historical record used thus far, 1968-1997, was split up into three time periods: 1968-1977 (10yrs.), 1977-1988 (12yrs.), and 1988-1997 (10yrs.), in order to study the sea ice and large scale climate interactions in each regime state separately. The PC1 time series was correlated with three month averaged periods (SON-MAM) of the SLP, SST and 500mb height gridded data, as described in the previous section. The results are summarized in the following sections. An analysis was first done using only two periods 1968-1977 and 1977-1997, but no significant large-scale patterns emerged in the second half of the record, thus motivating this new three period approach.

5.1 Correlation Patterns of SST

The three panels in Figure 8 show the SST correlations with PC1, from top to bottom, for the first (1968-'77), second (1977-'88) and third (1988-'97) periods. While there was little change in the patterns throughout the fall, winter and spring seasons, the highest correlations for the first and second periods occurred in DJF and for the last period in SON. In all cases the

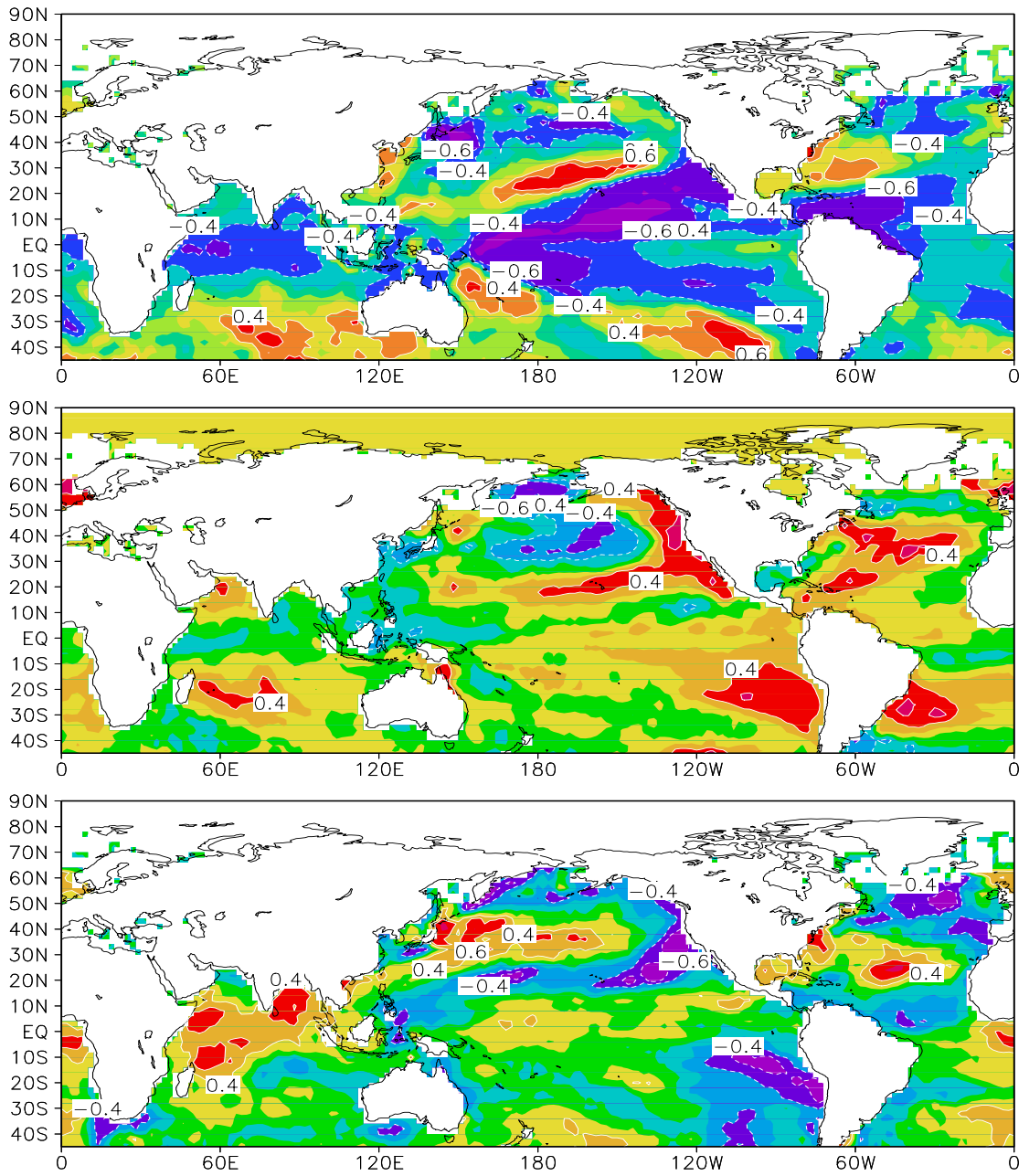


Figure 8: Correlation Patterns of SST

Correlations of gridded SST data and PC1 (JFM). The first period, 1968-1977 (DJF), is in the top panel; the second period, 1977-1989 (DJF), in the middle panel; and the third period, 1989-1997 (SON), in the bottom panel.

correlations are highest when SST anomalies lead the sea ice anomalies. The patterns in each period are quite different implying changing relationships between global SST anomalies and North Pacific sea ice between 1968 and 1997.

For the most part local sea surface temperatures are consistent with sea ice concentration. In all three periods, greater than average sea ice concentrations in the Bering Sea are highly correlated with cooler sea surface temperatures in the southern part of the sea. Similarly in the Sea of Okhotsk, for the first and last periods, below average sea ice extent is correlated with warmer waters at the edge of the sea.

Surprisingly, in the first period (Panel 1), below average sea ice concentrations in the Sea of Okhotsk are strongly correlated with anomalously cooler water at the extremity of the sea. Because it was found in previous sections that the sea ice dipole does not adequately address high and low ice years in the Sea of Okhotsk this result may not be contradictory. The Sea of Okhotsk time series in Figure 4 does show some years with greater than average sea ice during the second period. However, one possible physical explanation is that strong anomalous southeasterlies across the Sea of Okhotsk could potentially keep the ice edge from advancing despite the cool ocean temperatures.

5.1.1 First Period (1968-1977)

The SST anomaly pattern in the first period most strongly resembles the negative phase of the decadal ENSO SST pattern (Zhang et al., 1997). SST anomalies in the Pacific are not confined to the tropics and are quite broad in structure. The cold tongue extends as far south as southern Chile and as far north as Washington State with the highest correlations in the central tropical Pacific.

During this period before the 1976 regime shift, above average sea ice concentrations in the Bering Sea occurred more frequently. The correlations show that high sea ice concentrations in the Bering Sea are related to anomalously cool water in the Tropical Pacific (La Nina). This result was also found by Niebauer (1989) in his study on the interactions between ENSO and Bering Sea ice concentrations.

5.1.2 Second Period (1977-1988)

In the second period the most dominant feature in the SST field is identified in the north Pacific, strong correlations (+0.4) in the sub-tropical region around 30N and 30S, this pattern strongly resembles the Pacific Decadal Oscillation. Here, above average sea ice concentrations in the Bering Sea are related to cold SSTs in the central north Pacific and warm SSTs surrounding the cold anomalous center in a horseshoe pattern to the east.

The relationship between North Pacific sea ice variability (as defined by the dipole pattern) and tropical Pacific SSTs is opposite to the first period. In the second period, although the correlations are weak, above average sea ice concentrations in the Bering are related to anomalously warm water in the equatorial Pacific (El Nino).

5.1.3 Third Period (1988-1997)

The global SST anomaly pattern in the third period appears to be the opposite of the first period. Where high sea ice concentrations in the first period are related to a mature La Nina, in the third period they are related to newly forming El Nino. High correlations in the North Pacific resemble the PDO but the Kuroshio Extension region seems to be highlighted.

An index of the wintertime Kuroshio Extension was calculated by averaging the area over 20-45N and 120-170E. The correlation between the Kuroshio index for the SON period and PC1 (JFM) is 0.63 (95%). This result is consistent with Fang and Wallace (1998), with the exception that their analysis was done at zero lag (JFM) for the period 1972-1989.

In the second period high sea ice concentrations in the Bering are related to the positive phase of the PDO while in the third period it is related to the negative phase of the PDO. Another difference between the first and third periods that is important to note is that in the first period sea ice appears to be closely tied to ENSO while in the third period correlations with the PDO are much higher.

These are interesting results because it is still under debate whether or not the climate system post-1989 in the North Pacific returned to its pre-1977 state. This analysis shows a difference in the relationship between sea ice and SST anomalies between these two periods; evidence that suggests the third period maybe be yet another climate state.

5.1.4 Correlations in Remote Ocean Basins

In all three panels high (low) ice cover in the Bering Sea (Sea of Okhotsk) is correlated with warm sea surface temperature anomalies in the subtropical to midlatitude Atlantic Ocean and cool sea surface temperatures around 50N in the Atlantic. Correlations between PC1 and SST were carried out at different lags for the whole period but no significant correlations emerged in the Atlantic. Correlations between PC1 and the North Atlantic Oscillation (NAO) at various lags for all time periods also yielded no significant results.

Strong correlations also showed up in the Indian Ocean. In period one (Figure 8, Panel 1) the positive phase of the dipole index is related to cold SST anomalies in the Indian Ocean. In the third period (Panel 3), the relationship is opposite, positive PC1 index is related to warm Indian Ocean SST anomalies.

5.2 Correlation Patterns of SLP

Lagged correlations for SLP and z500 gridded data sets were calculated with the principal component of the first EOF to see if a mechanism could be outlined that ties SST anomalies with the North Pacific sea ice anomalies. One possible mechanism is as follows. In the tropics, where the ocean forces the atmosphere, anomalous sea surface temperatures could induce a Rossby wave train in the upper atmosphere. Variability in tropical SSTs could then impact variability in North Pacific (midlatitudes) where to the first order the atmosphere forces the ocean and sea ice.

To ease the discussion, mean sea level pressure fields for each period are shown in Figure 9. For the first two periods the Jan-Feb-Mar average is used and for the third period the Oct-Nov-Dec average is used. All three patterns are very similar. The main features are a center of low pressure over the North Pacific, the Aleutian Low, and a center of high pressure over Siberia, the Siberian High. After the regime shift in 1977 (Figure 8, Panels 2 and 3), the center of the Aleutian Low shifted eastward and deepened. Also a strengthening of the Siberian High after 1977 is noticeable in Figure 9.

Figure 10 shows the results of the SLP correlations. Highest correlations were found one month following the period of highest SST correlations. Panels 1 and 2 in Figure 10 are the

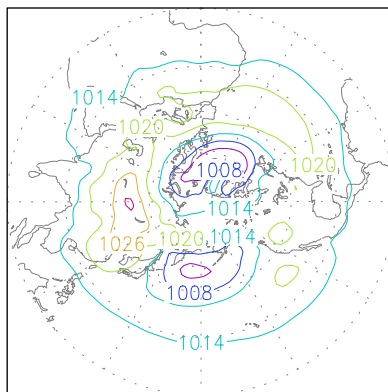
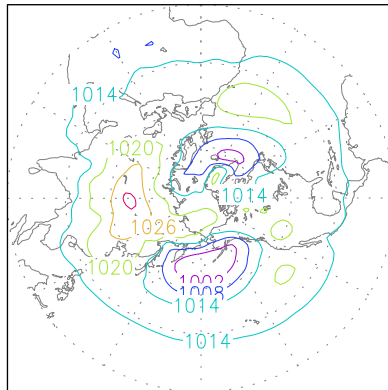
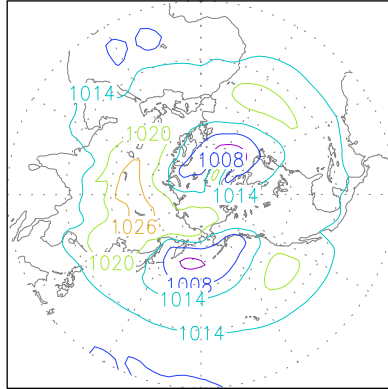


Figure 9: Patterns of Average SLP
 Average SLP field (mb) for each period. Top panel is period 1 (1968-1977) for DJF, middle panel is period 2 (1977-1989) for DJF and the bottom panel is period 3 (1989-1997) for OND.

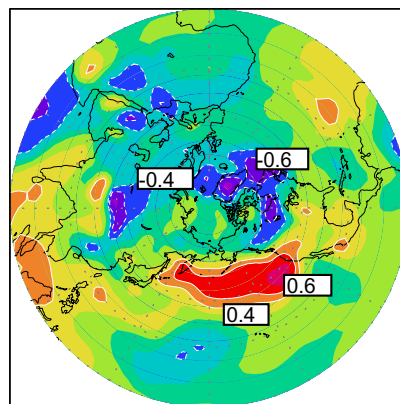
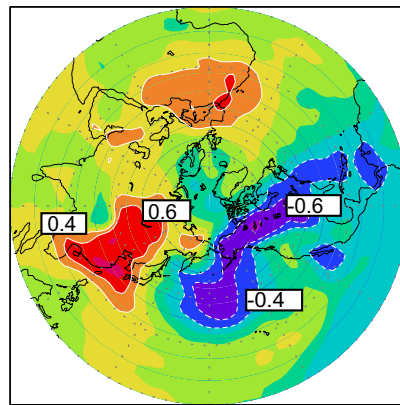
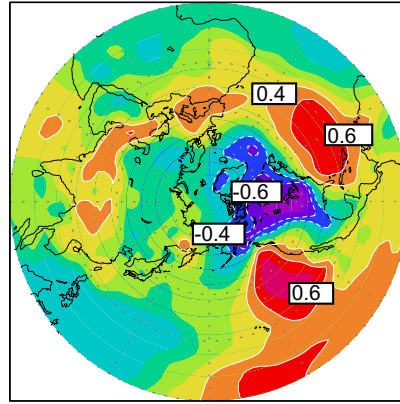


Figure 10: Correlation Patterns of SLP
 Correlations of gridded SLP data and PC1 (JFM). The first period (JFM) is in the top panel, the second period (JFM) in the middle panel and the third period (OND) in the bottom panel.

SLP correlations for the first two periods (JFM) and panel 3 is the SLP correlation for the third period (OND). In all three periods, cold air advection and warm air advection from anomalous geostrophic winds explain the sea ice anomalies. This atmospheric forcing of the sea ice is described in detail in the following section. In the first two periods there is no lag between the periods of highest SLP correlations and sea ice variability (JFM). This is consistent with Thorndike and Colony (1982) who found that sea ice can respond within days to geostrophic wind forcings. What is puzzling is that in the third period the highest correlations with the SLP field are when SLP leads the sea ice by three months. Because the sea ice responds to changes in the atmosphere on a timescale of days, it is unclear why the strongest correlations with sea level pressure would occur with such a long lead.

5.2.1 First Period

The dominant features in the first period are an anomalous low pressure zone over all of North America and two centers of high pressure, one in the sub-tropical Pacific situated off the west coast of North America, the other in the tropical Atlantic.

The low pressure over Alaska and high pressure over Siberia just north of the Sea of Okhotsk both force cool northerly continental air over the Bering Sea leading to above average ice extent, while the high pressure over the Sea of Okhotsk forces warm easterly ocean air over the Sea of Okhotsk restricting the advection of the ice edge.

5.2.2 Second Period

A large anomalous low pressure zone over all of North America also shows up in the second period. Unlike the first period however, the low pressure zone spills over into the Gulf of Alaska. A significant high pressure anomaly is present over Japan and southeastern Siberia.

The strengthened Aleutian Low causes anomalous northerly winds to travel across the Bering Sea (more ice) and anomalous easterlies across the Sea of Okhotsk (less ice).

5.2.3 Third Period

In the third period anomalous low pressure is only found in the eastern part of North America and unlike the first two periods, the center of low pressure extends over the North Atlantic.

The other dominant feature in this period is a weakened Aleutian Low across the whole North Pacific extending into the Gulf of Alaska and as far south as the coast of Washington State and California.

The weakened Aleutian Low causes anomalous southerly winds across the sea of Okhotsk and cold continental westerlies across the Bering Sea. The case for geostrophic winds forcing sea ice is weakest in this period because the anomalous winds are east-west and not north-south. Also, as mentioned earlier, the SLP leads the sea ice by 3 months. It is not clear with such a long lead time, how the SLP anomalies and sea ice anomalies are related.

5.3 Correlation Patterns of 500mb Height

Thus far, SST anomaly patterns have been identified that relate to the sea ice dipole during each period in the record. It appears that the response to tropical SST anomalies shows up a month later in mid-latitude SLPs which then force the sea ice. In this section a 500mb height gridded data set is correlated at various lags to see if any teleconnection patterns associated with the sea ice dipole emerge.

In each period the highest correlations occurred in the same time period and regions as the SLP anomalies. In all three periods, tropical SST anomalies correspond both geographically and in sign with the 500mb height anomalies. Cold (warm) SST anomalies cause a cooling (warming) of the atmosphere, higher (lower) pressure and lower (higher) 500mb heights.

Centers of action in the 500mb height field also occur over the North Pacific and are of the same sign as the SLP anomalies. It is possible that the SST anomalies in the tropics initiate a Rossby wave train that induces a pattern of 500mb height anomalies with a center over the North Pacific. In the tropics the ocean may be forcing the atmosphere and in the North Pacific some of the variability in the atmosphere that is forcing sea ice growth and sea surface temperatures may have its origins in the tropical Pacific Ocean (Niebauer, 1998). The timing of the correlations with the SST field and z500 field for the first two periods support this notion.

In the third period there is a three month lag between correlations in the atmosphere and sea ice anomalies. A mechanism that explains the lead-lag relationship between the atmosphere and sea ice is suggested and explored in section 5.3.3. Because sea ice can respond to

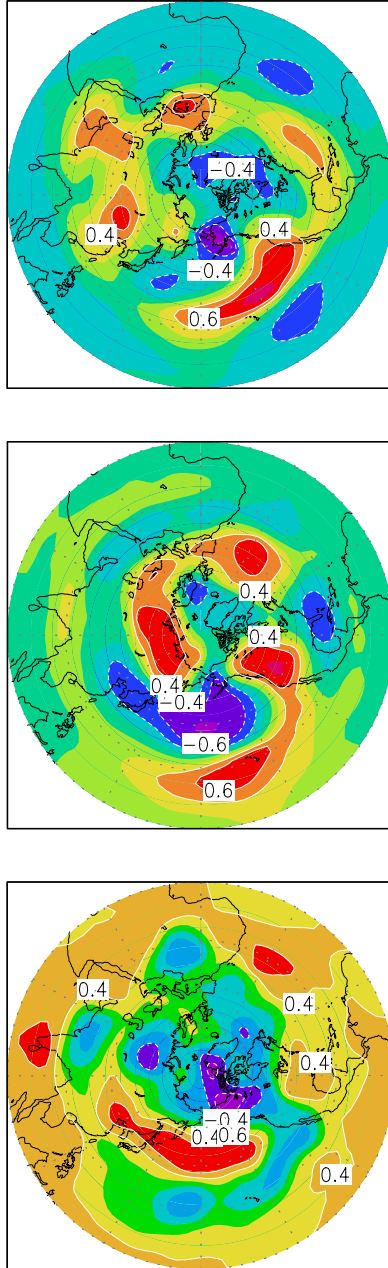


Figure 11: Correlation Patterns of z500
 Correlations of gridded 500mb height data and PC1 (JFM). The first period (JFM) is in the top panel, the second period (JFM) in the middle panel, and the third period (OND) in the bottom panel.

geostrophic winds in a short a time as a few days (Thorndike and Colony, 1982), it is unlikely that geostrophic winds associated with anomalous SLP patterns, leading the sea ice by three months, are forcing the sea ice anomalies.

5.3.1 First Period

The 500mb height pattern in the first period has characteristics of the negative phase of the Pacific North American teleconnection pattern (PNA). This teleconnection pattern can be defined as the leading EOF of the Northern Hemisphere 500mb height field. In Figure 11, a positive center over the east mid-latitude Atlantic, a negative center over the Arctic, a positive center off the western coast of North America and a weak negative center over the tropical Pacific together resemble a negative PNA like pattern. The positive center off the West Coast of California is southeast of the standard position of the North Pacific positive center in the negative PNA pattern, which is usually in the region of the Aleutian Low. The negative center over the Bering Sea usually resides over Alaska and Western Canada in the typical negative PNA pattern.

Cool ocean temperatures in the tropics could initiate or reinforce the PNA, beginning with the negative center, or anomalously low 500mb heights over the tropical Pacific. Niebauer (1989) discussed that it is through the PNA pattern that Tropical SST anomalies force North Pacific atmospheric anomalies and sea ice anomalies. The relative strengths and positions of the Aleutian Low and Siberian High may be controlled, in part, by the PNA pattern. As seen in the previous section, it is anomalous geostrophic winds from the Aleutian Low and Siberian High that force local sea ice anomalies.

5.3.2 Second Period

In the second period the 500mb height pattern resembles a classic positive phase of the winter-time PNA pattern associated with warm water in the equatorial Pacific (Horel and Wallace, 1981). The pattern is in the opposite phase of period one, which is consistent if it is responding to warmer SST anomalies in the tropical Pacific. As in the first period, it is possible that the PNA pattern has some influence on the position and strength of both the Aleutian Low and the Siberian High.

A relationship between the PNA pattern, ENSO and the Aleutian Low has been investigated by Niebauer (1989). He found that after the regime shift in 1977 the relationship between tropical SST's and the sign of the PNA switched. In this study the sign of the PNA associated with cool tropical SST anomalies remains consistent but there is a shift in the North Pacific lobe of the pattern. The resulting influence on North Pacific sea ice is the same for a changing phase in the PNA pattern after 1977 (Niebauer, 1989) and the shifting of the centers of action in the PNA found in this study.

A strong correlation in the 500mb height field over Asia may be evidence of an Asian connection (see section on Eurasian Snow Effects). Unlike the relationship between ENSO and the PNA, the relationship between the PNA and the Siberian High is not as well established. A possible Eurasian Snow forcing of the Siberian High is presented in section 6.

5.3.3 Third Period

The pattern in the third period is the typical West Pacific (WP) pattern (Wallace and Gutzler, 1981) characterized by a centre of action that extends from the west coast of Japan across the mid-latitude Pacific and another center of action of opposite sign over the North Pacific. The centre of high 500mb heights is consistent with SST anomalies in the Kuroshio Extension region where warmer waters may be causing rising motion and higher 500mb heights. In this study highest correlations with sea ice were found with SLP and 500mb heights lagging the SST field, implying an ocean forcing. This is consistent with (Battisti et al., 1995) who found in the Comprehensive Ocean Atmosphere Data Set (COADS) observations that the ocean flux anomalies are such that it appears the ocean is forcing the atmosphere in the regions of the Gulf Stream, however, elsewhere in the midlatitude North Atlantic it appears as though the atmosphere is forcing the ocean.

A positive West Pacific pattern, as seen in Panel 3 of Figure 12, is associated with a weaker Aleutian Low and a southward displaced storm track (Wallace and Gutzler, 1981). Overland and Pease (1982) found that as the North Pacific storm track is displaced northward (southward) sea ice concentrations in the Bering Sea decrease (increase). The results of these papers are consistent with the SLP and z500 correlations in this study. The positive West Pacific pattern (Figure 12, Panel 3) is positively correlated with the PC1 index, or above average sea ice concentrations in the Bering Sea. The Aleutian Low in the SLP correlations (Figure 11,

Panel 3) is weakened and is consistent with a southward displaced storm track, (Overland and Pease, 1982) which is associated with more sea ice in the Bering Sea. The mean position of the storm track is along the Aleutian Islands; if the storm track is displaced to the south there will be fewer storms in the Bering Sea that might break up the ice pack.

Correlations between the SLP fields and the 500mb height fields were highest when the atmosphere lagged the sea ice by three months. Niebauer (1998) found similar results when he correlated the West Pacific pattern with North Pacific sea ice anomalies and found the highest correlations with the sea ice lagging by up to two months.

6 Eurasian Snow Effect

The 500mb height correlations (Figure 11) for all three periods show varying activity over Asia characterized by a strong Siberian High and increased sea ice concentrations in the Bering Sea. The strongest is in the second period (Figure 11b) where there is a strong center of positive correlations in the region of the Siberian High. Other studies have found (Cohen, 2001) that snow cover extent in Eurasia in the fall can have an impact on wintertime northern hemisphere weather patterns.

PC1 was correlated with the snow cover data set at various lags for each of the periods. Because similar patterns (not shown) were found for each period, the analysis was repeated for the whole record (1971-1994, limited by the snow cover data set). Evidence of the 1977 and 1989 regime shifts appear to be confined to the North Pacific Ocean so it reasonable to assume they do not effect North Pacific variability which may be originating in Asia.

Lagged correlations between the gridded snow data set and PC1 were calculated for SON,OND,NDJ and DJF. Highest correlations were found in DJF where the snow extent (DJF) leads sea ice anomalies (JFM) by one month. An index of Eurasian snow extent was created for the whole record by averaging snow cover over the region 85-118E, 40-50N. This region was chosen because snow extent in this area had particularly high correlations with PC1, -0.55 (99).

The index of snow extent was correlated with the gridded sea level pressure data set at various lags. The highest correlations were also found at lag 0 (DJF). When there is increased snow

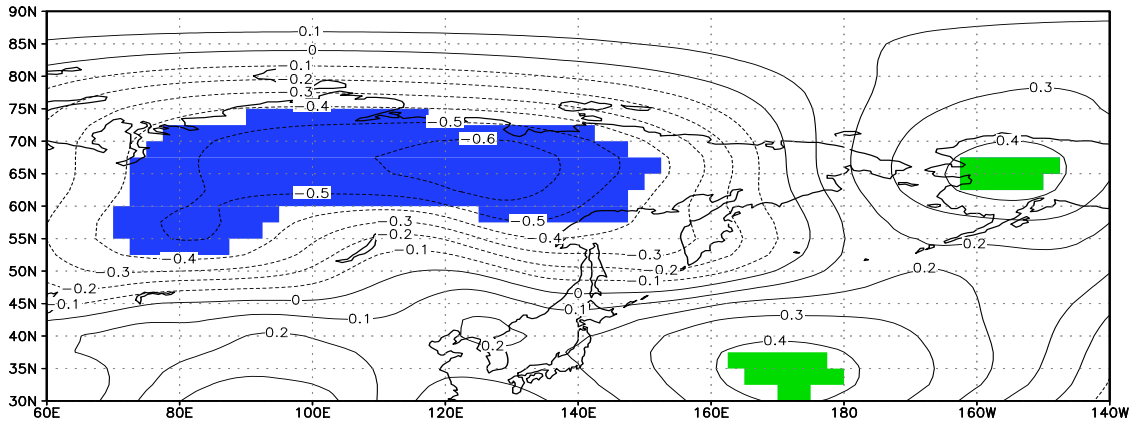


Figure 12: Correlation Pattern of Snow Index and z500

Snow index (DJF) correlated with z500 (DJF). The shaded regions represent a significance greater than 95% using a t-test.

cover in the index region then EOF1 of North Pacific Sea ice concentration is in its negative phase (less ice in the Bering Sea, more ice in the Sea of Okhotsk). Correlations between snow-cover index and the SLP field are consistent with a negative phase of the dipole index. Anomalous geostrophic winds associated with the high pressure anomalies over the mid-North Pacific and the low pressure over Siberia cause an advance of the ice edge in the Sea of Okhotsk and a retreat in the ice edge in the Bering Sea.

However, it is perplexing that increased snow cover in Eurasia is correlated with a weaker Siberian High. Increased snow-cover cools the lower atmosphere by decreasing the surface temperatures; this result was reproduced by correlating the Eurasian snow index with gridded SAT data. It was expected that higher surface pressures would result as air descends in the region of anomalously low surface temperatures.

The index of snow extent was also correlated with the z500 gridded data set at various lags. The highest correlations occurred at lag 0 (Figure 13). A center of low 500mb heights is consistent with an atmospheric column that is anomalously cool. Negative anomalies (low heights) in the 500mb height field are also consistent with cooler surface temperatures.

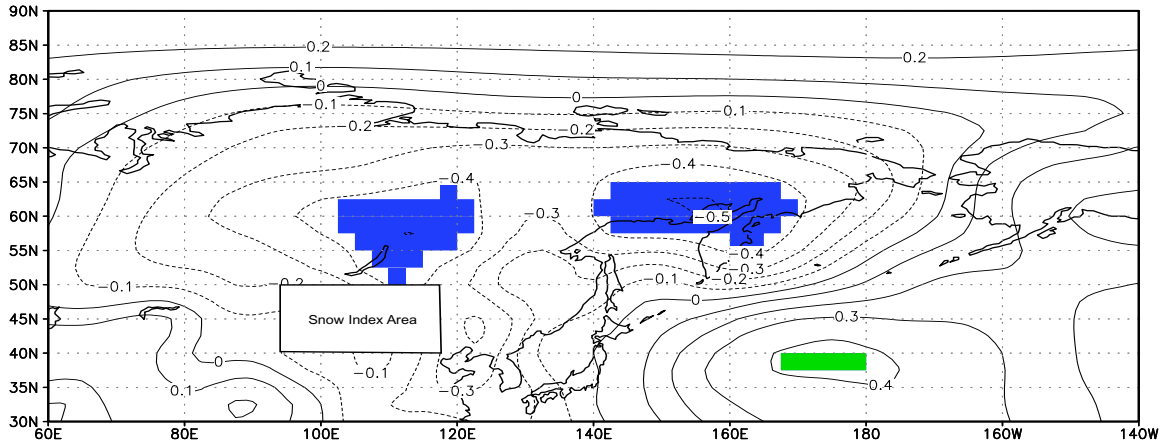


Figure 13: Correlation Pattern of Snow Index and SLP

Correlations between index of snow cover (DJF) and gridded sea level pressure (DJF). The shaded regions represent a significance greater than 95% using a t-test.

7 Synthesis

The PC1 time series was correlated with the major climate indices and Eurasian snow cover at various lags. Table 3, summarizes these results; only the maximum correlations are shown, with season of maximum correlation and significance in brackets. Because the snow cover data set only spans 1971-1995, correlations between the PC1 and snow cover index were not calculated for the three periods. The snow cover index and PC1 correlated at -0.55 (99) for the whole record (1971-1995).

In period one, correlations between PC1 and both the gridded SST data sets and the SOI index (Table 3) show a strong relationship between the North Pacific sea ice dipole and ENSO. Strongest correlations were found when the sea ice lags by one month implying a possible tropical forcing of the dipole pattern. The presence of the Pacific North American pattern in the DJF z500mb height correlations could be the mechanism by which variability from the tropical Pacific is transferred to the North Pacific. Following this reasoning, ENSO could explain 38% of the variability in the sea ice dipole for period 1 (0.62^2 , correlation from table 3). The possible Eurasian snow forcing that was discussed in the previous section for the whole period, could explain 30% of the variability in the dipole pattern.

	SOI	PDO
PC1(1968-1977)	0.62(95,DJF)	
PC1(1977-1988)		0.62(95,DJF)
PC1(1988-1997)		-0.74(95,OND)

Table 3: Correlations of PC1 and Climate Indices

Correlations of PC1 (JFM) and climate indices, no significant results were obtained for correlations with the NAO and AO.

Period two showed a strong relationship between the dipole pattern and the PDO one month earlier; these two time series correlate at 0.62 (Table 3). The PNA pattern in the 500mb height suggests a tropical connection although correlations with tropical SST's and the SOI index were low. To quantify, 38% of the variability in the dipole pattern can be explained by the main mode variability in North Pacific sea surface temperatures, the Pacific Decadal Oscillation. As in the other two periods 30% of the variability could be from Eurasian snow-cover.

Period three also showed a strong relationship between the dipole and the PDO. However, the sense of the relationship is opposite and the period of highest correlation in Oct-Nov-Dec. This could be because sea ice anomalies in this period may be responding to a change in the position of the storm track as opposed to anomalous wind forcing associated with SLP anomalies. Eurasian snow-cover one month earlier and the PDO (OND) together could account for 55% and 30% of the variability respectively.

8 Conclusion

The seesaw pattern in North Pacific sea ice that is generally used to describe the main mode of variability in North Pacific sea ice was reproduced in this study. Both the magnitude of the EOF pattern and correlations between the PC1 and the full sea ice data for the North Pacific were significantly larger in the Bering Sea. Further analysis of North Pacific sea ice variability, using correlations and composites, showed that the dipole pattern explains the majority of the interannual variability of sea ice in the Bering Sea but does not adequately address interannual variability of sea ice in the Sea of Okhotsk.

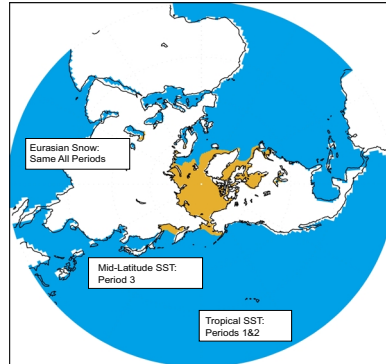


Figure 14: Origins of Possible Sea Ice Variability

It was found that with the regime shifts that the North Pacific Ocean underwent during 1977 and 1989, the relationships between North Pacific sea ice and the large-scale climate variability changed. Figure 14 summarizes the geographic locations of regions that covary with North Pacific sea ice. Before 1989 there is evidence of Tropical Pacific forcing of the sea ice which is stronger in the first period than in the second period. After 1989 there is no evidence of tropical Pacific forcings and a possible mid-latitude forcing was found to occur. For all three periods there is evidence of an Eurasian snow forcing of the sea ice anomalies.

In Period 1 the sea ice dipole pattern is strongly related to Tropical Pacific SSTs one month earlier. Correlations with northern hemisphere sea level pressure and 500mb heights, support the notion that Tropical Pacific SSTs may be influencing North Pacific sea ice through the PNA. Cooler SSTs in the Tropics may be inducing a Rossby wave train (PNA pattern in 500mb height) that forces anomalies in the lower atmosphere in the North Pacific. Correlations with SLP in the first period resulted in lower sea level pressures over Alaska; geostrophic winds associated with this low pressure would bring cooler continental air over the Bering Sea thus advancing the ice edge.

In Period 2, correlations with Northern Hemisphere 500mb heights also resulted in the PNA pattern. However, in Period 2 greater than average sea ice concentrations in the Bering Sea are correlated with warmer SSTs in the Tropical Pacific. Although the correlations between PC1 and Tropical Pacific SSTs are low, the strong PNA pattern in the 500mb height correlation, suggests that warm anomalies in Tropical Pacific SSTs may be inducing a positive PNA pattern

which would strengthen the Aleutian Low. The position of the low SLP anomalies in the North Pacific, and the associated geostrophic winds, would cause increased sea ice concentrations in the Bering Sea. High correlations between PC1 and the PDO in the second period suggest a strong link between variability in North Pacific sea ice and decadal variability in North Pacific SSTs.

In the third period, high correlations between PC1 and SSTs three months earlier in the region of the Kuroshio Extension, may be evidence of a mid-latitude Pacific SST forcing. It is postulated that warmer waters in the Kuroshio region may be inducing the positive West Pacific pattern in the 500mb height field that shows up one month later in the correlations with PC1. A positive phase of the West Pacific pattern has been associated with a weakened Aleutian Low and a southward shift in the mean position of the storm tracks (Wallace and Gutzler, 1981). A southward shift in the storm tracks, whose mean position is along the Aleutian Islands, would reduce the number of storms in the Bering Sea. Fewer storms in the Bering Sea could be associated with increased sea ice concentrations in this region because high winds caused by the passing of low pressure systems breaks up the ice pack.

In all three preperiods there is evidence of a Eurasian snow cover forcing of North Pacific sea ice anomalies. Decreased sea ice in the Bering Sea is related to increased snow cover in Eurasia. Correlations with the Eurasian snow cover index showed that increased snow cover is related to cooler surface air temperatures in Northern Eurasia and a weakened Siberian High. Geostrophic winds associated with the weakened Siberian High could cause a retreat of the ice edge in the Bering Sea.

The sea ice data set used in this study (1968-1997) was split into three separate periods. Different relationships between the sea ice anomalies and large-scale atmospheric and oceanic anomalies were found for each period. It is always a possibility that correlations with climate indices and remote anomalies in atmospheric and oceanic fields do not have any physical meaning. In this case, it is possible that the Tropical Pacific, mid-latitude Pacific and Eurasian snow connections are fortuitous and do not influence North Pacific sea ice. Although I do not believe this is true, it is always a possibility.

As more data become available, particularly sea ice concentration data in the Sea of Okhotsk, it will be easier to identify both low and high frequency variability in North Pacific sea ice. Model studies could also be useful to help distinguish between forcings and responses, something that is difficult to do with monthly averaged observational data.

9 Appendix A: List of Abbreviations

AO	Arctic Oscillation
CRU	Climate Research Unit
COADS	Comprehensive Ocean Atmosphere Data Set
DJF	December-January-February Average
ENSO	El Nino Southern Oscillation
EOF	Empirical Orthogonal Function
GICE	Global Sea Ice Content
JFM	January-February-March Average
MIZ	Marginal Ice Zone
mb	millibar
NAO	North Atlantic Oscillation
PC1	Principal Component time series associated with the first EOF pattern
PDO	Pacific Decadal Oscillation
SLP	Sea Level Pressure
SOI	Southern Oscillation Index
SST	Sea Surface Temperature
SVD	Singular Value Decomposition
UKMO	United Kingdom Meteorological Office
z500	500 millibar height

References

- [1] Baldwin, M. P. and T. J. Dunkerton, 1999: Propagation of the Arctic Oscillation from the stratosphere to the troposphere. *J. Geophys. Res.*, **104**, 30937-30946.
- [2] Battisti, D. S., and U. S. Bhatt, 1995: A modeling study of the interannual variability in the wintertime North Atlantic Ocean. *J. Climate*, **8**, 3067-3083.
- [3] Cavalieri, D. J. and Parkinson, C. L., 1987: On the Relationship Between Atmospheric Circulation and the Fluctuations in the Sea Ice Extents of the Bering and Okhotsk Seas. *J. Geophys. Res.*, **92**, 7141-7162.
- [4] Cohen, J., 2001: The Influence of Snow Cover on Northern Hemisphere Climate Variability. *Atmosphere-Ocean*, **39**, 35-53.
- [5] Fang, Z. and Wallace, J., 1994: Arctic Sea Ice Variability on a Timescale of Weeks and Its Relation to Atmospheric Forcing. *J. Climate*, **7**, 1897-1913.
- [6] Fang, Z. and Wallace, M., 1998: North-Pacific Sea Ice and Kuroshio SST Variability and Its Relation to the Winter Monsoon. *Polar Meteorol. Glaciol.*, **12**, 58-67.
- [7] Deser, C., J. Walsh, and M. Timlin, 2000: Arctic Sea Ice Variability in the Context of Recent Atmospheric Circulation Trends. *J. Climate*, **13**, 617-633.
- [8] Horel, J. and Wallace, J., 1981: Planetary-Scale Atmospheric Phenomena Associated with the Southern Oscillation. *Mon. Wea. Rev.*, **109**, 813-826.
- [9] Hare, S. and Mantua, J., 2000: Empirical Evidence for North Pacific Regime Shifts in 1977 and 1989. *Progress in Oceanography.*, **47**, 103-145.
- [10] Mantua, N., S. R. Hare, Y. Zhang, J. Wallace, R. Francis, 1997: A Pacific Interdecadal Climate Oscillation with Impacts on Salmon Production. *Bull. of the Meteor. Soc.*, **78**, 1069-1079.
- [11] Niebauer, H. J., 1989: Causes of Interannual Variability in the Sea Ice Cover of the Eastern Bering Sea. *GeoJournal*, **18.1**, 45-59
- [12] Niebauer, H. J., 1998: Variability in Bering Sea Ice Cover as Affected by a Regime Shift in the North Pacific in the Period 1947-1996. *J. Geophys. Res.*, **13**, 717-737.

- [13] Overland, J. and Pease, C., 1982: Cyclone Climatology of the Bering Sea and Its Relation to Sea Ice Extent. *Mon. Wea. Rev.*, **110**, 5-13.
- [14] Raynar, N.A. et al., 1996: Version 2.2 of the Global Sea Ice and Sea Surface Temperature data set, 1903-1994 by Raynar, N.A., Horton, E.B., Parker, D.E., Folland, and Hackett, R.B., 1996, CRTN44, Available from Hadley Center, Meteorological Office, Bracknell, UK.
- [15] Reynolds, R.W., and T.Smith, 1995: A High Resolution Global Sea Surface Temperature Climatology. *J. Climate*, **8**, 449-463.
- [16] Smith, N. R., R. W. Reynolds, R. E. Livezey, and D. C. Stokes, 1996: Reconstruction of historical sea surface temperatures using empirical orthogonal functions, *J.Climate*, **9**, 1403-1420.
- [17] Tachibana, Y., 1996: The Abrupt Decrease of the Sea Ice over the Souther Part of the Sea of Okhotsk in 1989 and Its Relation to the Recent Weakening of the Aleutian Low, *J. Meteor. Soc. Japan*, **74**, 579-584.
- [18] Trenberth, K. and Hurrell, J., 1994: Decadal Atmosphere-Ocean Variations in the Pacific. *Climate Dyn.*, **9**., 303-319.
- [19] Thorndike, A. S. and Colony, R., 1982: Sea Ice Motion in Response to Geostrophic Winds. *J. Geophys. Res.*, **87**, 5845-5852.
- [20] Wallace, J.M. and Gutzler, D.S.: Teleconnections in the Geopotential Height Field During the Northern Hemisphere Winter. *Mon. Weather Rev.*, **109**, 784-812.
- [21] Wilks, D.S. 1995: *Statistical Methods in the Atmospheric Sciences*. 121-122. Academic Press, Inc.
- [22] von Storch, H. and F. Zwiers, 1999: *Statistical Analysis in Climate Research*. Cambridge University Press, Cambridge UK, 484pp.
- [23] Zhang, Y.J., M.Wallace and D. S. Battisti, 1997: ENSO-like interdecadal variability. *J.Climate*, **10**, 1004-1020.